Testing for memory-free spectroscopic coordinates by 3D IR exchange spectroscopy

Borek, Joanna A ; Perakis, Fivos ; Hamm, Peter

Abstract: Using 3D infrared (IR) exchange spectroscopy, the ultrafast hydrogen-bond forming and breaking (i.e., complexation) kinetics of phenol to benzene in a benzene/CCl4 mixture is investigated. By introducing a third time point at which the hydrogen-bonding state of phenol is measured (in comparison with 2D IR exchange spectroscopy), the spectroscopic method can serve as a critical test of whether the spectroscopic coordinate used to observe the exchange process is a memory-free, or Markovian, coordinate. For the system under investigation, the 3D IR results suggest that this is not the case. This conclusion is reconfirmed by accompanying molecular dynamics simulations, which furthermore reveal that the non-Markovian kinetics is caused by the heterogeneous structure of the mixed solvent.

DOI: https://doi.org/10.1073/pnas.1406967111

Testing for memory-free spectroscopic coordinates by 3D IR exchange spectroscopy

Joanna A. Borek [*], **Fivos Perakis** [*] **and Peter Hamm** [*]

[*]Department of Chemistry, University of Zurich, Winterthurerstr. 190, CH-8057 Zürich, Switzerland

Submitted to Proceedings of the National Academy of Sciences of the United States of America

Using three dimensional infrared (3D IR) exchange spectroscopy, the ultrafast hydrogen-bond forming and breaking (i.e., complexation) kinetics of phenol to benzene in a benzene/CCl_4 mixture is investigated. By introducing a third time-point at which the hydrogen-bonding state of phenol is measured (in comparison to 2D IR exchange spectroscopy), the spectroscopic method can serve as a critical test whether the spectroscopic coordinate used to observe the exchange process is a memory-free, or Markovian, coordinate. For the system under investigation, the 3D-IR results suggest that this is not the case. This conclusion is reconfirmed by accompanying molecular dynamics simulations, which furthermore reveal that the non-Markovian kinetics are caused by the heterogenous structure of the mixed solvent.

Significance Statement: When the speed of a chemical reaction becomes as fast as the relaxation of its solvent, the Markovian assumption is likely to break down. In this case, the probability of a reaction to happen at a given time point does not only depend on the current state of the molecular system itself, but also on the memory that persist within the solvent. The Markovian assumption is nevertheless essentially always made, because deviations from Markovianity are difficult to determine experimentally. 3D IR exchange spectroscopy provides a very sensitive test of Markovianity, which, in turn, opens important insights on how solvents influence or even control the course of chemical reactions.

Introduction

Whenever one writes a chemical reaction equation, such as in the simplest case that of an equilibrium between two states of a molecular system:

$$C \rightleftharpoons F \qquad [1]$$

with the corresponding Master equation for its kinetics:

$$\begin{aligned}\frac{d[C]}{dt} &= -k_{CF}[C] + k_{FC}[F] \\ \frac{d[F]}{dt} &= +k_{CF}[C] - k_{FC}[F],\end{aligned} \qquad [2]$$

one implicitly assumes Markovianity. That is, it is assumed that the probability to react per time unit e.g. from C to F scales linearly with concentration $[C]$ with proportionality constant k_{CF}, but does *not* depend on the history of how C has been formed. When the reaction is slow in comparison to the relaxation of its environment, then this assumption is well justified. One can however think of many situations where this is not the case. For example, proteins are heterogeneous on very long timescales due to their structural complexity, so enzymatic reaction catalyzed by them might not fulfill that condition [1]. Other examples are found in glass-forming liquids close to the glass transition, when their relaxation covers many orders of magnitude in time [2].

When the speed of a reaction approaches the ultrafast picosecond regime, which is the topic of the present paper, then even the solvation time of normal liquids far away from any glass transition may become time-limiting. For example it has been shown that the distance between a Na^+ and a Cl^- ion is not a good reaction coordinate to describe ion pair dissociation in aqueous solution [3], in the sense that the distance for which the free energy peaks does not correspond to the transition state of the reaction. Hidden coordinates exist, which must be solvent coordinates since there aren't any other degrees of freedom. Unless these solvent coordinates haven't fully relaxed and lost their memory about a reaction event, the probability for a back reaction must depend on the history. Markovianity is related to a separation of timescales between the speed of a chemical reaction of a molecular system versus that of the relaxation of its solvent. Often, a separation of timescales goes hand-in-hand with a separation of solute and solvent, but such a system-bath approach fails for ultrafast reactions.

It is important to recognize that the question of Markovianity is not an intrinsic property of a chemical process, but rather is related to its level of description and/or observability. When resorting to a full phase space description of solute together with the solvent as a limiting scenario, any system would be Markovian as it follows deterministic Newtonian mechanics. However, since such a high-dimensional description is not practical for complex solution phase systems, one typically tries to find lower-dimensional reaction coordinates to describe a process, along which the dynamics is not necessarily Markovian. If one approaches a problem from molecular dynamics (MD) simulations, in which case full phase space knowledge is in principle available in the background, one can try to design "good" reaction coordinates, where "good" refers to the question whether or not the dynamics is Markovian along these coordinates. This however is a notoriously difficult problem [4, 5]. For protein folding, Markov state models do get close to that point [6], but for ion pair dissociation discussed above [3], for example, this goal has not been achieved since solvent coordinates would have to be included. In real life spectroscopy, the situation becomes even worse since one does not have full phase space knowledge and the reaction coordinate is dictated by the spectroscopic method, with little or no freedom for the experimenter to design a good reaction coordinate. We will call the readout of the spectroscopy used in an experiment a "spectroscopic coordinate". There is no guarantee whatsoever that such a spectroscopic coordinate is

Reserved for Publication Footnotes

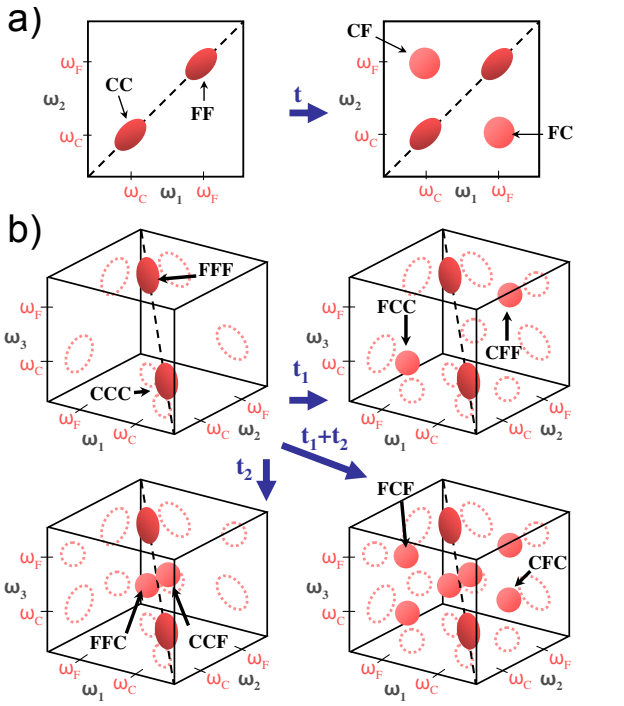

Fig. 1. Sketch of a) diagonal and cross peaks in a 2D IR exchange experiment. At short waiting time t, only diagonal peaks (CC and FF) are present. Upon increasing t, cross peaks CF and FC emerge. b) Diagonal and cross peaks in a 3D IR exchange experiment. At short t_1 and t_2 population times only two diagonal peaks corresponding to unchanged species C and F are present (CCC and FFF). Upon increasing t_1 and/or t_2, cross peaks emerge (CCF, FFC, FCC, CFF, CFC and FCF). The dotted lines show the projections of the 3D IR peaks onto the ω_{12}, ω_{13} and ω_{23} planes.

Markovian, and it is the topic of this paper to experimentally test whether or not it is.

If a process is Markovian along a given reaction coordinate, then the 3-time-point joint probability function $p(k, t_2+t_1|j, t_1|i, 0)$ to be in state k at time t_2+t_1, provided the system was in state i at time 0 and in state j at time t_1 (where i, j, k is either C or F), factorizes into two identical 2-time-point joint probability functions $p(j, t_1|i, 0)$ [7]:

$$\begin{aligned} p_{ijk}(t_1, t_2) &\equiv p(k, t_2+t_1|j, t_1|i, 0) \\ &= p(k, t_2|j, 0) \cdot p(j, t_1|i, 0). \end{aligned} \qquad [3]$$

While Eq. 3 is the general criterion for Markovianity, when reducing the probability functions to functions of discrete binary coordinates $\{i, j, k\} = \{C, F\}$, then Eq. 3 results in a two-state system Eq. 2 with exponential solutions, *i.e.*, a Poissonian process.

2D exchange spectroscopy measures directly the 2-time-point joint probability function, and its realization in the IR spectral range can do so on very fast, picosecond timescales [8, 9, 10, 11, 12, 13, 14, 15, 16, 17, 18, 19, 20]. In such an experiment, the frequency of a vibrational mode, which can distinguish the two states C or F of a molecular system, is considered to be the spectroscopic coordinate. A spectrum of the molecular system is measured twice, separated by a waiting time t, and plotted along two frequency axes ω_1 and ω_2 (Fig. 1a). The first frequency measurement labels states C or F via its vibrational frequency. If the waiting time t is set to zero, then all molecules will still be in the same state C or F for the second frequency measurement and thus reveal the same vibrational frequency. Consequently, the 2D IR spectrum will contain only diagonal peaks (Fig. 1a, left). When

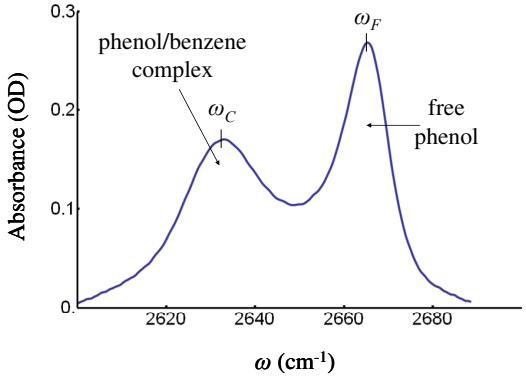

Fig. 2. Absorption spectrum of deuterated phenol in a mixed benzene/CCl_4 solvent with two peaks: the OD-stretch vibration of a phenol-OD/benzene complex at 2631 cm^{-1} (ω_C) and that of free phenol-OD at 2666 cm^{-1} (ω_F).

increasing the waiting time t, some of the molecules will react between both measurements, so they will reveal different frequencies giving rise to off-diagonal peaks, or cross peaks, in the 2D IR spectrum (Fig. 1a, right). The time dependence of diagonal and cross peaks, in essence, reflects the 2-time-point joint probability function $p(j, t|i, 0)$.

Here, we extend exchange spectroscopy by one more frequency dimension. 3D optical spectroscopy has been realized for other applications both in the IR [21, 22, 23, 24, 25, 26] and the visible [27, 28, 29, 30, 31, 32] (for reviews see Refs. [33, 34]). In 3D exchange spectroscopy, the vibrational frequency of a molecule is measured three times along axes ω_1, ω_2 and ω_3, separated by two waiting times t_1 and t_2. In analogy to 2D IR spectroscopy, a 3D IR spectrum shows only the two diagonal peaks along the body-diagonal at (ω_C, ω_C, ω_C) and (ω_F, ω_F, ω_F) when both waiting times t_1 and t_2 are set to zero (Fig. 1b, top left). When increasing these waiting times and exchange events take place, cross peaks show up. There are in total six possibilities for cross peak in a 3D IR exchange spectrum, appearing on the off-diagonal corners of a cube spanned by (ω_C, ω_F). If scanning t_1 only (Fig. 1b, top right), the (ω_C, ω_F, ω_F) and (ω_F, ω_C, ω_C) cross peaks may show up, while the (ω_C, ω_C, ω_F) and (ω_F, ω_F, ω_C) cross peaks are revealed for t_2 (Fig. 1b, bottom left). In addition, if scanning both waiting times, double exchange cross peaks (ω_C, ω_F, ω_C) and (ω_F, ω_C, ω_F) might become observable (Fig. 1b, bottom right). In full analogy to 2D exchange spectroscopy, the time dependence of diagonal and cross peaks reflects the 3-time-point joint probability function $p(k, t_2+t_1|j, t_1|i, 0)$, which, in turn, can test Markovianity via Eq. 3. That very idea has been formulated for 3D-NMR exchange spectroscopy already quite some time ago [35], but has not been realized as of yet, to the best of our knowledge not for 3D-NMR, and certainly not for 3D IR spectroscopy.

For the purpose of this study, we chose the complexation (*i.e.*, hydrogen-bonding) of deuterated phenol to benzene in a benzene/CCl_4 mixture as a model system. The spectroscopic coordinate to distinguish the two states of phenol, complexed (C) *versus* free (F), is the vibrational frequency of the OD-stretch vibration, since hydrogen-bonding causes a frequency red shift of $\sim$35 cm^{-1}. Consequently, the stationary IR absorption spectrum shows two discrete peaks centered at frequencies ω_C and ω_F (Fig. 2), the integrated intensities of which represent the equilibrium constant. 2D IR exchange spectra of that molecular system have been presented by Fayer and coworkers [11, 12] with a hydrogen bond dissociation time of $\approx$8 ps.

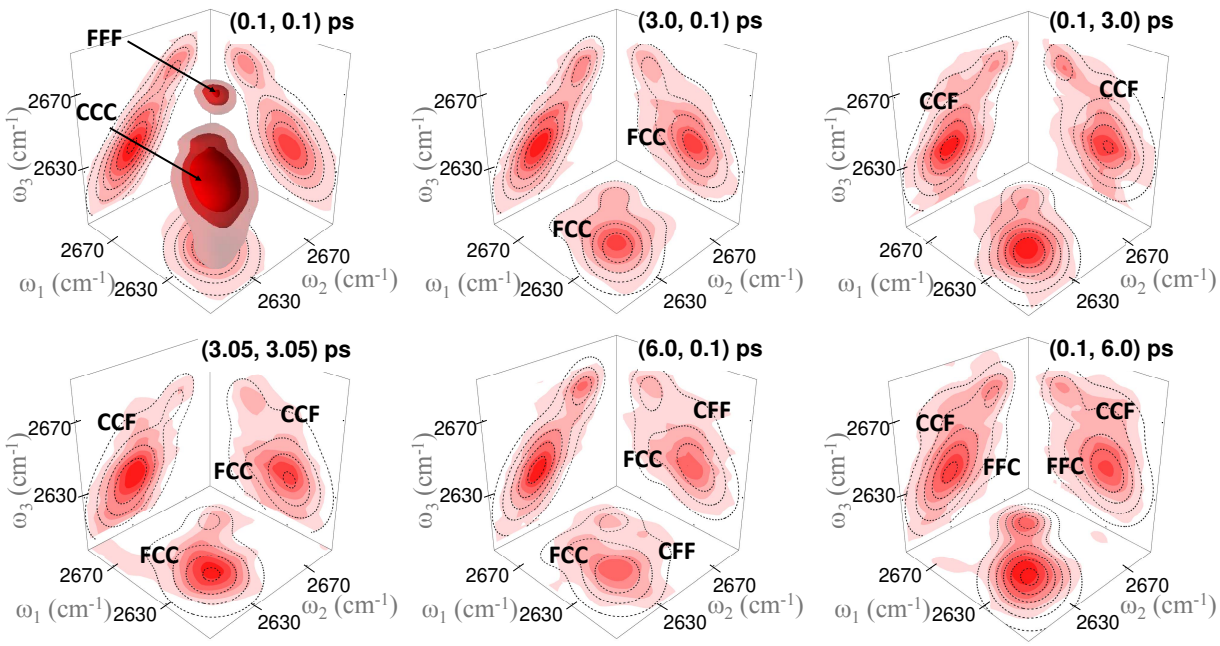

Fig. 3. 3D IR spectra of phenol/benzene complexation at various population times (t_1, t_2). The (0.1, 0.1) ps spectrum is shown fully in three dimensions, the other spectra only as projections onto the ω_{12}, ω_{23} and ω_{13} planes. Experimental data are shown in red, fits to the data in black. Emerging cross peaks are assigned.

Accompanying molecular dynamics (MD) simulations [13] have suggested that the mixed benzene/CCl_4 solvent is not homogeneous and forms clusters of certain sizes that predominantly consist of either benzene or CCl_4. A phenol molecule thus can either be inside one of these clusters and be fully surrounded by benzene or CCl_4, respectively, or at a boundary between clusters (see Fig. 12 of Ref. [13]). In the first case, the probability of an exchange event is expected to be small, as the phenol molecule has to first diffuse out of the corresponding cluster. In the second case, exchange is probably faster since the molecule just has to turn around. The spectroscopic coordinate senses hydrogen bonding but cannot distinguish whether the molecule has diffused into one of these clusters or sits at a boundary. Hence, along that coordinate, the probability of an exchange event at a given time point could be expected to depend on the history of a particular phenol molecule. 2D IR exchange spectroscopy, however, is not a sensitive probe of two-state behavior, and consequently deviations from it have not been discussed explicitly in Refs. [11, 12, 13]. In the present paper, we demonstrate that 3D IR spectroscopy is a sensitive probe of two-state dynamics, and we show that the hydrogen bond exchange of phenol in benzene/CCl_4 indeed is not a two-state process.

Results

Experimental Results. Fig. 3, red contours, shows the measured 3D IR spectra of phenol/benzene complexation for various t_1 and t_2 population times. As in 2D IR exchange [11, 12], the spectroscopy of this molecular system is particularly simple, because the 1-2 and 2-3 transitions, which would complicate the interpretation [8, 10], are shifted completely out of the spectral window due to the large anharmonicity of the OD-vibrator. We therefore have to consider only the $0 \rightarrow 1$ transition in all of the following discussion. The 3D data are shown only for the earliest population times (t_1=0.1, t_2=0.1) ps, whereas for later population times we display the projections onto the ω_{12}, ω_{13} and ω_{23} planes. In this way, we avoid hiding spectral features because of perspective effects and, as a side aspect, increase the signal-to-noise ratio somewhat due to further averaging along the different axes. At the same time, for the $2^3 = 8$ peaks in a 3D IR exchange spectrum, these three projections with $3 \times 2^2 = 12$ possible peaks contain the full information (Fig. 1b).

At short population times, (t_1=0.1, t_2=0.1) ps, only two peaks are visible on the diagonal, one corresponding to free phenol (FFF) and the other to a phenol-benzene complex (CCC). The asymmetry in peak size comes from the relatively large ratio of extinction coefficients for the complexed and free phenol species, $\epsilon_C/\epsilon_F = 2.3$ [11]. To compensate for its small extinction coefficient, we had chosen a relatively high concentration of uncomplexed phenol so its peak is larger in the 1D absorption spectrum (Fig. 2), but since the 3D IR signal size scales as ϵ^3, it ends up to be smaller in Fig. 3.

Upon increasing the population times t_1 and t_2, cross peaks emerge in the spectra, which appear as elongations of the diagonal peaks since the two vibrators are rather close in frequencies. When increase t_1 only, as for the (3.0, 0.1) and (6.0, 0.1) ps spectra, exchange can happen during the first

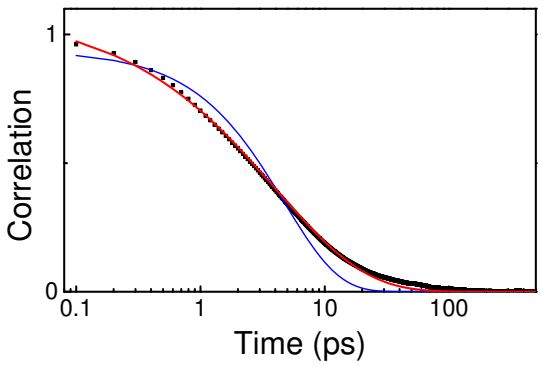

Fig. 4. Correlation function as defined in Eq. 4 (black squares), together with an exponential (blue line) and a stretched exponential fit (red line).

and not the second population time. Therefore a cross peak FCC appears, corresponding to a free phenol that complexed during t_1. The counterpart of that situation is the CFF cross peak for a phenol/benzene complex that dissociated during t_1. This cross peak can be barely seen in the (3.0, 0.1) ps spectrum, since it is much less intense than the FCC cross peak due to the extinction coefficient difference, but it becomes visible in the longer t_1=6.0 ps case. When scanning t_2 without t_1, see the (0.1, 3.0) and (0.1, 6.0) ps spectra, exchange occurs during t_2 only. This leads to cross peaks CCF and FFC, the latter, again, visible essentially only in the (0.1, 6.0) ps spectrum.

When both population times are scanned, as in the (3.05, 3.05) ps spectrum, the cross peaks already discussed for the (3.0, 0.1) and (0.1, 3.0) ps spectra (CCF and FCC) now both appear. In principle, also the double exchange cross peaks FCF and CFC should show up in this spectrum, but they are too weak to be detected with our current signal-to-noise ratio.

Molecular Dynamics Results. In order to guide the interpretation of the experimental results, we performed MD simulations of the system, following essentially the protocol of Ref. [13] with adjusted concentrations of the various molecular components to better match the experiment (see Material and Methods). Based on an order parameter that determines whether or not the phenol molecule is hydrogen bonded at a given instant of time during the MD trajectory (see Supplementary Material Sec. SI and Fig. S1), we calculated the correlation function:

$$c(t) = \frac{\langle \delta H(t) \delta H(0) \rangle}{\langle \delta H^2 \rangle} \qquad [4]$$

where $H(t)$ is a binary function that is either 0 or 1 for free or complexed phenol, respectively. In the above equation, $\delta H(t) \equiv H(t) - \langle H \rangle$ and $\langle H \rangle$ is the average of $H(t)$. Fig. 4 shows the correlation function, which is surprisingly long-lived extending beyond 100 ps with the present signal-to-noise ratio, and decays in a highly non-exponential manner. That is, the blue line shows the best exponential fit $\propto \exp(-t/\tau)$, revealing a time constant of τ=5 ps, and the red line a stretched exponential fit $\propto \exp(-(t/\tau)^{\beta})$ with a stretching factor of β=0.6 and a characteristic time τ=4 ps. The latter reveals a significantly better fit, but is still not perfect, in particular for the long-time tail. In any case, the extracted timescale

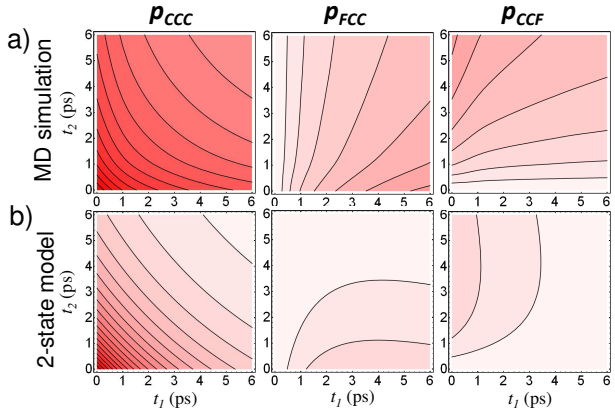

Fig. 5. 3-time point joint probability functions p_{CCC}, p_{FCC} and p_{CCF} deduced from a) the MD simulation and b) the two-state model which uses parameters deduced from 2D IR spectroscopy [11]. Contour lines are in steps of 5% of the peak signal of p_{CCC}.

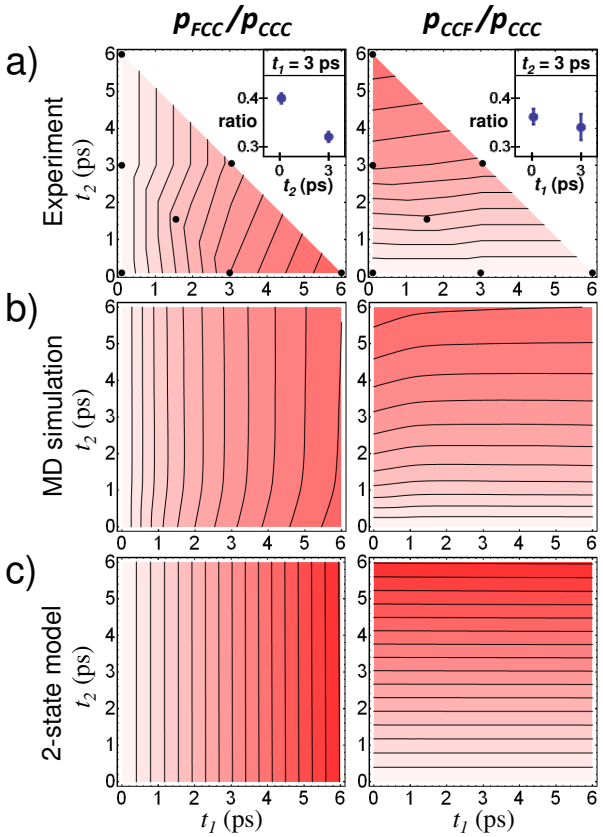

Fig. 6. Ratios p_{CCF}/p_{CCC} and p_{FCC}/p_{CCC} for a) experimental 3D IR data b) MD simulation and c) two-state model. Contour lines are in steps of 0.05 and are the same for all three plots. The dots in panel (a) mark the positions where 3D IR spectra have been taken. The insets of panel (a) show the ratios p_{FCC}/p_{CCC} and p_{CCF}/p_{CCC} along t_2 and t_1, respectively, with the corresponding other time coordinate fixed to 3.0 ps.

is in essentially quantitative agreement with the experimental value [11, 12].

Fig. 5a exemplifies some of the 3-time point joint probability functions p_{CCC}, p_{FCC} and p_{CCF} calculated from $H(t)$. As expected, p_{CCC} decreases as a function of t_1 and t_2, whereas p_{FCC} and p_{CCF} increase with t_2 and t_1, respectively. It can be seen that p_{FCC} and p_{CCF} are symmetric with respect to interchanging t_1 and t_2, a symmetry which can be verified on general grounds from the time-reversibility of an equilibrium ensemble. Independent from that, the time-dependence of these 3-time point joint probability functions is rather complex and it is not obvious *per se* whether or not they follow two-state dynamics.

Discussion

In order to test whether the experimental and MD results follow two-state dynamics, a simple test can be deduced from Eq. 3. That is if the process was two-state, then one would obtain e.g for the ratio p_{FCC}/p_{CCC}:

$$\begin{aligned} \frac{p_{FCC}}{p_{CCC}} &\equiv \frac{p(C, t_1 + t_2 | C, t_1 | F, 0)}{p(C, t_1 + t_2 | C, t_1 | C, 0)} \\ &= \frac{p(C, t_2 | C, 0) \cdot p(C, t_1 | F, 0)}{p(C, t_2 | C, 0) \cdot p(C, t_1 | C, 0)} = \frac{p(C, t_1 | F, 0)}{p(C, t_1 | C, 0)}, \end{aligned} \qquad [5]$$

which is a function of t_1 only. As such, contour lines in a 2D plot of that ratio are expected to be vertical (Fig. 6, left col-

umn). In other words, the probability of staying in C during time t_2 does not depend on the history of the system during time t_1. Likewise, the ratio p_{CCF}/p_{CCC} is a function of t_2 only, and the contour lines are expected to be horizontal (Fig. 6, right column).

To illustrate that criterion, we first constructed a two-state model, which assumes that the 3D IR response can be pieced together from two 2D IR responses, and which includes the effects of exchange as well as vibrational relaxation and orientational diffusion on the level of rate equations in order to describe the peak intensities (see Supplementary Material, Sec. SII and SIII and Fig. S2 for details). For the parameters, we used the ones deduced from 2D IR spectroscopy [11]: hydrogen bond dissociation rate $1/k_{CF}$=8 ps, vibrational relaxation times for free and complexes phenol T_1^F=12.5 ps and $1/T_1^C$=10 ps, respectively, and orientational relaxation times τ_r^F=2.9 ps and τ_r^C=3.4 ps. Since we had chosen a smaller benzene concentration in order to enlarge the free phenol peak, the ratio of complexed to free phenol was smaller [complex]/[free]=0.6 than in Ref. [11], and the complexation rate $k_{FC} = k_{CF} \cdot$ [complex]/[free] was adjusted accordingly.

Fig. 5b shows 3-time point joint probability functions p_{CCC}, p_{FCC} and p_{CCF} of the two-state model, which are equally complex as those from the MD simulations (Fig. 5a), but in detail quite different. Most of these differences originate from the fact that the two-state model does include in addition vibrational relaxation and rotational diffusion, which affect the sizes of the 3D IR peaks as well. Despite the complex time-dependencies of the 3-time point joint probability functions, the ratios p_{FCC}/p_{CCC} and p_{CCF}/p_{CCC} simplify significantly (Fig. 6c), and indeed, the contour lines are either vertical or horizontal, respectively, as expected from the Markovian criterion Eq. 5. (Very careful analysis in fact reveals a minor deviation from that behavior, which is not visible on the scale of Fig. 6c. This effect is related to orientational diffusion discussed in Supplementary Material, Sec. SII). The corresponding ratios p_{FCC}/p_{CCC} and p_{CCF}/p_{CCC} from the MD simulation, on the other hand, deviate significantly from Eq. 5 at early times (Fig. 6b). Fig. S3 (Supplementary Material) shows that deviations from two-state dynamics persist also for much longer times, in agreement with the slow tail in the correlation function (Fig. 4).

With these results in mind, we return to the discussion of the experimental results. In order to extract a quantity that is directly comparable to the simulation results, we fitted the 3D IR spectra with multivariate Gaussians for each diagonal and cross peak (black contour lines in Fig. 3) and thereby extracted their volumes (see Supplementary Material, Sec. SIV, for details). Since the various spectra of Fig. 3 have been measured at different days, their overall signal intensity varies significantly and plotting the absolute values analogous to Fig. 5 turned out not to be meaningful. But the ratios of Fig. 6 cancel out these day-to-day variation, and furthermore, allow one to test two-state behavior. Indeed, the contours are tilted very much like those from the MD simulation, and hence the hydrogen-bond exchange kinetics of phenol in benzene/CCl_4 is concluded not to follow two-state dynamics. The essential information lies in the comparison of the (3.0, 3.0) ps point with the (0.1, 3.0) ps and (3.0, 0.1) ps points, which is highlighted in Fig. 6a together with error bars. In particular ratio p_{FCC}/p_{CCC} varies as a function of times t_2 beyond experimental error, in contrary to what would be expected from Eq. 5 if the process would follow two-state dynamics. It is furthermore reassuring that the MD simulations qualitatively reproduce the experimental results, both in terms of the direction of the tilts as well as their size.

The upward tilt of the contour lines of p_{CCF}/p_{CCC} (Fig. 6a, right) means that if the system already stayed in C for a longer time t_1, the likelihood to switch during t_2 is reduced. That interpretation is consistent with the cluster picture deduced from MD simulations [13]. That is, if a phenol molecule has already proven to be complexed for a long time during t_1, it likely is inside one of the benzene cluster, and thus the probability for its hydrogen bond to break is smaller. The tilt of the vertical contour lines of p_{FCC}/p_{CCC} towards the right (Fig. 6a, left) can be explained in a similar manner.

Concluding Remarks

In the case of two discrete states (Eq. 1), non-exponential kinetics is already a good indication of non-Markovianity, in the sense that Eq. 2 should reveal an exponential response. The multiple timescales contained in the stretched exponential function needed to fit the two-timepoint correlation function Eq. 4 (Fig. 4) reflect the heterogenous structure of the mixed benzene/CCl_4 solvent [13], with a probability for hydrogen-bond exchange that depends on where a phenol molecule is situated in that heterogenous solvent. 2D IR exchange spectroscopy, in essence, measures that two-timepoint correlation function. However, in practice, in the presence of experimental noise as well as when other kinetic processes such as vibrational relaxation contribute, it is often very difficult to distinguish exponential from non-exponential response; the data in Refs. [11, 12] would probably not allow one to do so. Hence the Markovian assumption is usually implicitly made, mostly since no critical test exists and not because it is necessarily very well justified. In the present paper, we demonstrate that 3D IR spectroscopy provides a sensitive test of Markovianity by introducing a third time point into the measurement. As such, the method can compare the kinetics between two of these time-points in dependence of the state the system during the third time-point. The analysis shows that the hydroxyl stretch frequency, which is the spectroscopic coordinate in this case and tests whether of not the hydroxyl group is hydrogen bonded, is not a Markovian coordinate.

The goal in analyzing complex systems is to find observables that make the description of a process Markovian [7]. In order to be able to do so, one needs a test of how good a given spectroscopic coordinate is, and 3D exchange spectroscopy can achieve exactly that.

ACKNOWLEDGMENTS. We thank the anonymous reviewer for pointing out a critical error in the data fitting. We furthermore thank Gerhard Stock for insightful discussions, Minhaeng Cho and Kijeong Kwac for making some of the force field details of Ref. [13] available to us, and Sean Garrett-Roe for help with the experimental setup in an early stage of the project. The work has been supported by the Swiss National Science Foundation (SNF) through the National Center of Competence and Research (NCCR) MUST.

Materials and Methods

3D IR Setup. The 3D IR setup has been introduced previously [24, 26, 22], including an active phase stabilization based on a HeNe tracer beam [36], polarization balanced detection [37] and scattering suppression achieved with two wobbling Brewster windows and a photoelastic modulator [38]. The pulses were passed through individual motorized translation stages and piezo actuators to independently control the τ_1, t_1, τ_2, t_2 and τ_3 delay times (where τ_i denote the coherence times and t_i the population times). The data were collected as a function of τ_1 and τ_2 coherence times and frequency ω_3 for a given set of population times t_1 and t_2 and

2D Fourier transformed with respect to τ_1 and τ_2 to yield (ω_1, ω_2, ω_3) spectra.

Due to the thick sample cell (100 μm, in comparison to 1-6 μm in other 3D IR measurements [24, 26, 22]), the phasing scheme implemented previously [39] could not be used. Alternatively, the phase has been determined such as to maximize the integral of the 3D IR spectrum. For this particular sample, this procedure is the most sensitive one, since only positive contributions are expected in the 2600-2700 cm^{-1} spectral window from the 0-1 transitions, while transitions higher up in the vibrational ladder with in part opposite signs [22] are outside of that window. A badly phased spectrum would result in the mixing in of dispersive contributions, *i.e.* it would cause negative bands to appear in the spectrum. Additionally, small phase errors induce quite significant shifts on the ω_3 axis. Again, since only the $0 \rightarrow 1$ transitions contribute to the 3D IR spectrum, the peak positions can directly be compared with those in the 1D absorption spectrum (Fig. 2), serving as a sensitive cross-check of the phasing procedure.

Sample Preparation. The system under investigation is phenol dissolved in a mixed benzene/CCl_4 solvent. Phenol-OD was used to shift the hydroxyl stretch vibration outside of the CH-stretch window. A molar ratio of 2:30:100 (phenol-OD : benzene : CCl_4) was used, revealing an absorbance of free and complexed phenol of 0.26 and 0.17 OD, respectively (Fig. 2). Phenol-OD was obtained by deuterating phenol-OH in methanol-OD. The solution was sandwiched between two CaF_2 windows with a 100 μm teflon spacer.

Molecular Dynamics Simulations. MD simulations where performed with essentially the same simulation protocol as Cho and coworkers [13]. That is, we used the OPLS-AA parametrization of CCl_4 [40] and the same partial charges and Lennard Jones parameters as Ref. [13] for benzene and phenol. One phenol molecule deuterated only at the hydroxyl group was dissolved in a simulation box containing 130 benzene molecules and 498 CCl_4 molecules (the benzene/CCl_4 ratio was chosen smaller than in Ref. [13] to better account for the experimental conditions). MD simulations were performed with the Gromacs program package [41] with a timestep of 2 fs, all bonds constrained, and a time constant of 0.5 ps for the thermostat. Lennard Jones interactions were treated with a cut-off of 1.0 nm (switching at 0.9 nm) and the long range electrostatic forces were treated by the Particle-Mesh-Ewald approximation. After an initial energy minimization and equilibration at 1 bar, production runs with a total length of 1.7 μs were collected in the NVT ensemble.

1. Brian P, E., Min, W., Antoine M, v., Lee, K. T., Luo, G., Hongye Sun aand Binny J, C., Kou, S. C., and Xie, X. S. Ever-fluctuating single enzyme molecules: Michaelis-Menten equation revisited. Nature Chem. Biol. 2, 87–94 (2006).
2. Schmidt-Rohr, K. and Spiess, H. W. Nature of nonexponential loss of correlation above the glass-transition investigated by multidimensional NMR. Phys. Rev. Lett. 66, 3020–3023 (1991).
3. Geissler, P. L., Dellago, C., and Chandler, D. Kinetic pathways of ion pair dissociation in water. J. Phys. Chem. B 103, 3706–3710 (1999).
4. Best, R. B. and Hummer, G. Reaction coordinates and rates from transition paths. Proc. Natl. Acad. Sci. USA 102, 6732–6737 (2005).
5. Krivov, S. V. and Karplus, M. Diffusive reaction dynamics on invariant free energy profiles. Proc. Natl. Acad. Sci. USA 105, 13841–13846 (2008).
6. Pande, V. S., Beauchamp, K., and Bowman, G. R. Everything you wanted to know about Markov state models but were afraid to ask. Methods 52, 99–105 (2010).
7. Van Kampen, N. G. Stochastic Processes in Physics and Chemistry. Elsevier, Amsterdam, (1992).
8. Woutersen, S., Mu, Y., Stock, G., and Hamm, P. Hydrogen-bond lifetime measured by time-resolved 2D-IR spectroscopy: N-methylacetamide in methanol. Chem. Phys. 266, 137–147 (2001).
9. Kwac, K., Lee, H., and Cho, M. Non-Gaussian statistics of amide I mode frequency fluctuation of N-methylacetamide in methanol solution: Linear and nonlinear vibrational spectra. J. Chem. Phys. 120, 1477–1490 (2004).
10. Kim, Y. S. and Hochstrasser, R. M. Chemical exchange 2D IR of hydrogen-bond making and breaking. Proc. Natl. Acad. Sci. USA 102, 11185–11190 (2005).
11. Zheng, J., Kwak, K., Asbury, J., Chen, X., Piletic, I. R., and Fayer, M. D. Ultrafast dynamics of solute-solvent complexation observed at thermal equilibrium in real time. Science 309, 1338–1343 (2005).
12. Kwak, K., Zheng, J., Cang, H., and Fayer, M. D. Ultrafast two-dimensional infrared vibrational echo chemical exchage experiments and theory. J. Phys. Chem. B 110, 19998–20013 (2006).
13. Kwac, K., Lee, C., Jung, Y., Han, J., Kwak, K., Zheng, J., Fayer, M. D., and Cho, M. Phenol-benzene complexation dynamics: Quantum chemistry calculations, molecular dynamics simulations, and two-dimensional IR spectrosocpy. J. Chem. Phys. 125, 244508 (2006).
14. Zheng, J. R., Kwak, K., Xie, J., and Fayer, M. D. Ultrafast carbon-carbon single-bond rotational isomerization in room temperature solution. Science 313, 1951–1954 (2006).
15. Sanda, F. and Mukamel, S. Stochastic simulation of chemical exchange in two dimensional infrared spectroscopy. J. Chem. Phys. 125, 014507 (2006).
16. Cahoon, J. F., Sawyer, K. R., Schlegel, J. P., and Harris, C. B. Determining transition-state geometries in liquids using 2D-IR. Science 319, 1820–1823 (2008).
17. Jansen, T. L. and Knoester, J. Waiting time dynamics in two-dimensional infrared spectroscopy. Acc. Chem. Res. 42, 1405–1411 (2009).
18. Anna, J. M., Ross, M. R., and Kubarych, K. J. Dissecting enthalpic and entropic barriers to ultrafast equilibrium isomerization of a flexible molecule using 2D IR chemical exchange spectroscopy. J. Phys. Chem. A 113, 6544–6547 (2009).
19. Ji, M., Odelius, M., and Gaffney, K. J. Large angular jump mechanism observed for hydrogen bond exchange in aqueous perchlorate solution. Science 328, 1003–1005 (2010).
20. Olschewski, M., Knop, S., Seehusen, J., Lindner, J., and Vöhringer, P. Ultrafast internal dynamics of flexible hydrogen-bonded supramolecular complexes. J. Phys. Chem. B 115, 1210–1221 (2011).
21. Ding, F. and Zanni, M. T. Heterodyned 3D-IR spectroscopy. Chem. Phys. 341, 95–105 (2007).
22. Garrett-Roe, S. and Hamm, P. Purely absorptive three-dimensional infrared spectroscopy. J. Chem. Phys. 130, 164510 (2009).
23. Garrett-Roe, S. and Hamm, P. Three-point frequency fluctuation correlation functions of the OH stretch vibration in liquid water. J. Chem. Phys. 128, 104507 (2008).
24. Garrett-Roe, S., Perakis, F., Rao, F., and Hamm, P. 3D-IR spectroscopy of isotope-substituted liquid water reveals heterogeneous dynamics. J. Phys. Chem. B 115, 6976–6984 (2011).
25. Mukherjee, S. S., Skoff, D. R., Middleton, C. T., and Zanni, M. T. Fully absorptive 3D IR spectroscopy using a dual mid-infrared pulse shaper. J. Chem. Phys. 139, 144205 (2013).
26. Perakis, F., Borek, J. A., and Hamm, P. Three-dimensional infrared spectroscopy of isotope-diluted ice Ih. J. Chem. Phys. 139, 014501 (2013).
27. Turner, D. B., Stone, K. W., Gundogdu, K., and Nelson, K. A. Three-dimensional electronic spectroscopy of excitons in GaAs quantum wells. J. Chem. Phys. 131, 144510–144510–8 (2009).
28. Fidler, A. F., Harel, E., and Engel, G. S. Dissecting hidden couplings using fifth-order three-dimensional electronic spectroscopy. J. Phys. Chem. Lett. 1(19), 2876–2880 (2010).
29. Davis, J. A., Hall, C. R., Dao, L. V., Nugent, K. A., Quiney, H. M., Tan, H. H., and Jagadish, C. Three-dimensional electronic spectroscopy of excitons in asymmetric double quantum wells. J. Chem. Phys. 135, 044510–044510–9 (2011).
30. Zhang, Z., Wells, K. L., and Tan, H.-S. Purely absorptive fifth-order three-dimensional electronic spectroscopy. Opt. Lett. 37(24), 5058–5060 (2012).
31. Li, H., Bristow, A. D., Siemens, M. E., Moody, G., and Cundiff, S. T. Unraveling quantum pathways using optical 3D Fourier-transform spectroscopy. Nature Commun. 4, 1390 (2013).
32. Chen, P. C., Wells, T. A., and Strangfeld, B. R. High-resolution coherent three-dimensional spectroscopy of Br_2. J. Phys. Chem. A 117, 5981–5986 (2013).
33. Garrett-Roe, S. and Hamm, P. What can we learn from 3D-IR spectroscopy? Acc. Chem. Res. 42, 1412–1422 (2009).
34. Cundiff, S. T. Optical three dimensional coherent spectroscopy. Phys. Chem. Chem. Phys. , DOI: 10.1039/c4cp00176a (2014).
35. Schmidt-Rohr, K. and Spiess, H. W. Multidimensional Solid-state NMR and Polymers. Academic Press Limited, London, (1994).
36. Volkov, V., Schanz, R., and Hamm, P. Active phase stabilization in Fourier-transform two-dimensional infrared spectroscopy. Opt. Lett. 30, 2010–2012 (2005).
37. Middleton, C., Strasfeld, D., and Zanni, M. Polarization shaping in the mid-IR and polarization-based balanced heterodyne detection with application to 2D IR spectroscopy. Opt. Express 17(17), 14526–14533 (2009).
38. Bloem, R., Garrett-Roe, S., Strzalka, H., Hamm, P., and Donaldson, P. Enhancing signal detection and completely eliminating scattering using quasi-phase-cycling in 2D IR experiments. Opt. Express 18(26), 27067–27078 (2010).
39. Backus, E. H. G., Garrett-Roe, S., and Hamm, P. Phasing problem of heterodyne-detected two-dimensional infrared spectroscopy. Opt. Lett. 33, 2665–2667 (2008).
40. Jorgensen, W. L. and Severance, D. L. Aromatic-aromatic interactions: Free energy profiles for the benzene dimer in water, chlorophorm and liquid benzene. J. A. Chem. Soc. 112, 4768–4774 (1990).
41. van der Spoel, D., Lindahl, E., Hess, B., Groenhof, G., Mark, A. E., and Berendsen, H. J. C. Gromacs; fast, flexible and free. J. Comput. Chem. 26, 1701–1718 (2005).